nature energy

PERSPECTIVE

https://doi.org/10.1038/s41560-019-0439-6

Manganese oxidation as the origin of the anomalous capacity of Mn-containing Li-excess cathode materials

Maxwell D. Radin*, Julija Vinckeviciute, Ram Seshadri and Anton Van der Ven*

The lithium-excess manganese oxides are a candidate cathode material for the next generation of Li-ion batteries because of their ability to reversibly intercalate more Li than traditional cathode materials. Although reversible oxidation of lattice oxygen has been proposed as the origin of this anomalous excess capacity, questions about the underlying electrochemical reaction mechanisms remain unresolved. Here, we critically analyse the O^{2-}/O^{-} oxygen redox hypothesis and explore alternative explanations for the origin of the anomalous capacity, including the formation of peroxide ions or trapped oxygen molecules and the oxidation of Mn. First-principles calculations motivated by the Li–Mn–O phase diagram show that the electrochemical behaviour of the Li-excess manganese oxides is thermodynamically consistent with the oxidation of Mn from the +4 oxidation state to the +7 oxidation state and the concomitant migration of Mn from octahedral sites to tetrahedral sites. It is shown that the Mn oxidation hypothesis can explain the poorly understood electrochemical behaviour of Li-excess materials, including the activation step, the voltage hysteresis and voltage fade.

Li-excess layered manganese oxides[1,2] have attracted widespread attention because of their large reversible capacity, which considerably exceeds that of conventional Li-ion cathode materials[3–5]. Li-excess materials are not only of commercial interest, but also raise fundamental scientific questions because their large reversible capacities cannot be explained by the conventional understanding of redox mechanisms in intercalation compounds. Conventional theories are also unable to explain other unusual electrochemical behaviour, including a 4.5 V 'activation' plateau during the first charge; a ~0.5 V hysteresis that persists even at low rates[1,6]; and a gradual decrease in the average voltage on cycling ('voltage fade')[7,8]. These features are rarely seen in other intercalation compounds, but appear almost universally across a wide range of layered Li-excess manganese oxides that includes layered Li_2MnO_3 (refs. [9–11]) and its alloys[1,2,12]. Similar behaviour is also seen in related compounds such as Mn-containing disordered rocksalts[13,14], Na-intercalated manganese oxides[15–18], and some 4*d* and 5*d* transition-metal oxides[19–24].

The most widely accepted interpretation of the anomalous capacity of Li-excess manganese oxides is reversible O^{2-}/O^{-} redox[25–29]. According to this hypothesis, the removal of Li results in the depletion of non-bonding oxygen *p* states, resulting in turn in the oxidation of O^{2-} ions to O^{-}. The experimental basis for this interpretation is the absence of evidence for transition-metal oxidation[14,26,28,30–34] and the appearance of a localized spectroscopic feature in the oxygen K-edge, which has been attributed to an O^{-} species[26,30,31,34].

Despite extensive study of Li-excess materials and the broad acceptance of the oxygen redox hypothesis, a detailed picture of how oxygen redox would lead to an activation plateau, hysteresis and voltage fade remains elusive. The migration of transition-metal ions to octahedral sites in the Li layer is widely understood to be involved in these phenomena[7,35,36]. It has been suggested that the coupling of oxygen redox to such transition-metal migration could explain the unusual electrochemical behaviour of Li-excess materials[30,37]. Nevertheless, although the electrochemical behaviour of conventional intercalation electrodes such as Li_xCoO_2 and Li_xFePO_4 can be described by rigorous thermodynamic and kinetic models[5,38], such models remain largely phenomenological for the Li-excess manganese oxides[39]. Furthermore, the spectroscopic feature attributed to O^{-} is consistent with molecular oxygen and peroxide ions[31,40–42]. These considerations motivate a re-examination of possible redox mechanisms in the Li-excess manganese oxides.

Here we critically analyse the experimental evidence for O^{2-}/O^{-} oxygen redox in Li-excess materials and show that other phenomena, such as the decomposition of the cathode material, can explain the observed spectroscopic features. We then explore alternative mechanisms, including the formation of peroxide ions or trapped oxygen molecules, and the oxidation of Mn^{4+} to Mn^{7+} with concomitant migration from octahedral to tetrahedral sites. Although a case for the reversible formation of molecular oxygen or peroxide ions has already been made[43–45], we argue that Mn^{4+}/Mn^{7+} redox (possibly in concert with the formation of peroxide ions or trapped oxygen molecules) should also be given serious consideration, as it is consistent with available experimental evidence and is capable of explaining the activation plateau, voltage hysteresis and voltage fade. We conclude by noting that there is insufficient experimental evidence to determine to what extent O^{2-}/O^{-} redox and each of the alternative mechanisms occurs, and that the fragility of cathode materials at high states of charge may be a major impediment to resolving how much each mechanism contributes to the anomalous capacity.

Critical analysis of oxygen redox

Although 'oxygen redox' can, in principle, refer to any redox process involving oxygen, the anomalous capacity of Li-excess manganese oxides is generally attributed to a specific oxygen redox mechanism: the reversible oxidation of lattice O^{2-} ions to O^{-} ions[25,26,29]. The removal of electrons from oxygen *p* states, rather than transition-metal *d* states, has been attributed to a specific local environment:

Materials Department, University of California Santa Barbara, Santa Barbara, CA, USA. *e-mail: maxradin@engineering.ucsb.edu; avdv@engineering.ucsb.edu

oxygen *p* states for which neither of the cation sites that the state points at is occupied by a transition-metal ion[25]. It is important to acknowledge that transition-metal oxides exhibit a high degree of covalency, and attributing redox to one particular species is a simplification. For example, prior calculations show that the charge density around oxygen ions changes during the deintercalation of $LiCoO_2$, despite the fact that this reaction nominally operates on the Co^{3+}/Co^{4+} redox couple[46,47]. Despite the subtleties arising from hybridization, formal oxidation states are a powerful tool in understanding intercalation chemistry. In particular, first-principles calculations show that the changes in electronic structure arising from the removal of Li from Li_2MnO_3 and other Mn^{4+} oxides (assuming no other structural rearrangement) can sensibly be interpreted as the reduction of O^{2-} to O^- (refs. [25,44]). (We emphasize that the O^{2-}/O^- oxygen redox mechanism is distinct from the oxygen redox mechanism suggested to occur during the delithiation of 4*d* and 5*d* transition-metal oxides, involving 'peroxo-like' O_2^{n-} species[19,22–24].)

Although the O^{2-}/O^- oxygen redox interpretation has been widely embraced as explaining the anomalous capacity of Li-excess manganese oxides[24,30,48–50], it represents a radical departure from the corpus of materials chemistry. Localized oxygen holes have been observed as radiation-induced point defects[51,52], but the notion of a material in which a macroscopic portion of oxygen sites can be interpreted as O^- ions is, to our knowledge, unprecedented. (Superconducting cuprates and rare-earth nickelates have been cited as a precedent[24,53], but these compounds are characterized by a high degree of covalency and generally are not construed to contain an O^- species[54,55].) Being an extraordinary claim, the O^{2-}/O^- oxygen redox interpretation of Li-excess manganese oxides requires extraordinary evidence.

The crux of the evidence for the oxygen redox hypothesis is the spectroscopic observation of localized, unoccupied oxygen *p* states. X-ray absorption spectroscopy shows the appearance of an absorption peak at 531 eV during the first-charge plateau of many different Li-excess manganese oxides[26,30,31,34,56]. Excitation near this energy yields emission at 523 eV (refs. [26,31,56]). That the emission at 523 eV is driven by absorption at 531 eV is especially evident in resonant inelastic X-ray scattering (RIXS) maps[30,31,57], demonstrating that these two features are localized to the same species. Similar absorption and emission features are also seen in Na manganese oxides that exhibit an anomalous capacity[16,17,58].

Although the appearance of localized spectroscopic features has been interpreted as the signature of O^{2-}/O^- redox, it is also consistent with the formation of molecular O_2 (ref. [41]), as noted by Xu et al.[31]. Similar spectroscopic features have been observed in lithium peroxide[40,59]. In contrast, simulated spectra of stretched peroxide molecules suggest[30] that an O^- species would not have an absorption feature near 531 eV. Although it has been suggested that molecular oxygen or peroxide ions are forming reversibly during electrochemical cycling[34,43–45], such species could also be the product of the irreversible decomposition of the cathode. This would not be surprising, given that the release of oxygen gas is typically favoured thermodynamically for oxide cathode materials at high states of charge[5,60]. Decomposition could, for example, occur spontaneously after the charged cathode is removed from the electrochemical cell for ex situ characterization. (To the best of our knowledge, all O K-edge measurements on Li-excess manganese oxides have been performed ex situ.) Decomposition could also be triggered by beam damage during spectroscopic experiments. That the changes in the oxygen spectrum are consistent with the formation of molecular O_2 or peroxide ions means that, despite widespread acceptance, there is no direct evidence that compellingly supports the O^{2-}/O^- oxygen redox mechanism in the context of Li-excess manganese oxides. Although the absence of direct evidence does not disprove the O^{2-}/O^- oxygen redox hypothesis, it motivates a critical re-examination of alternative reaction mechanisms.

Exploration of alternative redox mechanisms

Several other mechanisms have been hypothesized to account for the anomalous capacity of the Li-excess manganese oxides, including the release and subsequent reduction of O_2 (ref. [61]), the formation of oxygen vacancies that enable $Mn^{2+}/Mn^{3+}/Mn^{4+}$ redox[62–65], the insertion of protons[10,66], the reversible formation of peroxide ions[34,43–45,67] and the oxidation of Mn beyond the +4 oxidation state[9,67]. In this analysis, we reconsider possible mechanisms, starting from basic thermodynamic considerations.

The first charge cycle, characterized by a 4.5 V plateau, provides a starting point for analysing possible redox mechanisms. Figure 1 shows the plateau during the first charge of various Li_2MnO_3–$LiMO_2$ composites[6,67] and pure Li_2MnO_3 (ref. [11]). (While it is still under debate as to whether such compounds are better described as a solid solution or a coherent two-phase mixture, we will refer to them as composites.) The sloping part of the voltage curve for the composite materials arises from the delithiation of the $LiMO_2$ component, whereas the plateau is associated with the Li_2MnO_3 component. The universality of the 4.5 V plateau is especially apparent in Fig. 1b, which compares the activation plateau of pure Li_2MnO_3 to that of the Li_2MnO_3 component of each Li_2MnO_3–$LiMO_2$ composite, obtained by removing the portion of the voltage curve that corresponds to the theoretical capacity of the $LiMO_2$ component and rescaling the composition axis.

Phase diagrams provide a starting point for understanding the reaction mechanisms that could occur during the activation plateau. The equilibrium pathway resides in the Li–*M*–Mn–O composition space. However, we can restrict ourselves to the Li–Mn–O phase diagram since the voltage and capacity of the activation plateau (relative to the fraction of 'Li_2MnO_3') is unaffected by the identity of the other transition metals *M* of the composite (Fig. 1), indicating that the activation plateau involves only the Li_2MnO_3 component. The relevant portion of the equilibrium Li–Mn–O phase diagram (as calculated by the Materials Project[68–70]) is shown in Fig. 2a. The equilibrium delithiation mechanism, represented by a dashed line, leads to the release of oxygen gas through the reactions

$$Li_2MnO_3 \rightarrow \frac{1}{5}Li_4Mn_5O_{12} + \frac{3}{10}O_2 + \frac{6}{5}Li^+ + \frac{6}{5}e^- \quad 3.72\,V \qquad (1)$$

and

$$Li_4Mn_5O_{12} \rightarrow 5MnO_2 + O_2 + 4Li^+ + 4e^- \quad 4.02\,V \qquad (2)$$

(Voltages are referenced to Li/Li^+ and are computed from data in the Materials Project[68–70].) Although such a 'densification' mechanism was initially thought to be responsible for the first-charge plateau[1,35,36], this pathway now seems unlikely because the amount of gas detected by differential electrochemical mass spectrometry (DEMS) during the first charge of Li_2MnO_3–$LiMO_2$ composites is far too small to account for the observed capacity[26,31,71].

The DEMS measurements cannot rule out the possibility that O_2 could remain trapped within the active material as isolated molecules[44] or small pockets of gas. If such trapped oxygen were reversibly reduced and oxidized on subsequent cycles, the cell would function as a 'hybrid Li-ion/Li–O_2' battery[72]. Alternatively, oxygen could be reversibly oxidized to form peroxide dimers. Early ex situ Raman[26,73] studies failed to detect peroxide ions or molecular oxygen, but recent in situ studies have observed a Raman peak consistent with peroxide ions[45]. First-principles calculations also indicate that the delithiation of Li-excess Mn oxides could potentially result in the formation of peroxide ions or trapped oxygen molecules[43,44].

While the reversible formation of peroxide ions or trapped oxygen molecules has been used to explain the anomalous capacity of Li-excess Mn oxides[34,43–45,67], here we explore an alternative mechanism that has received little consideration: the oxidation of

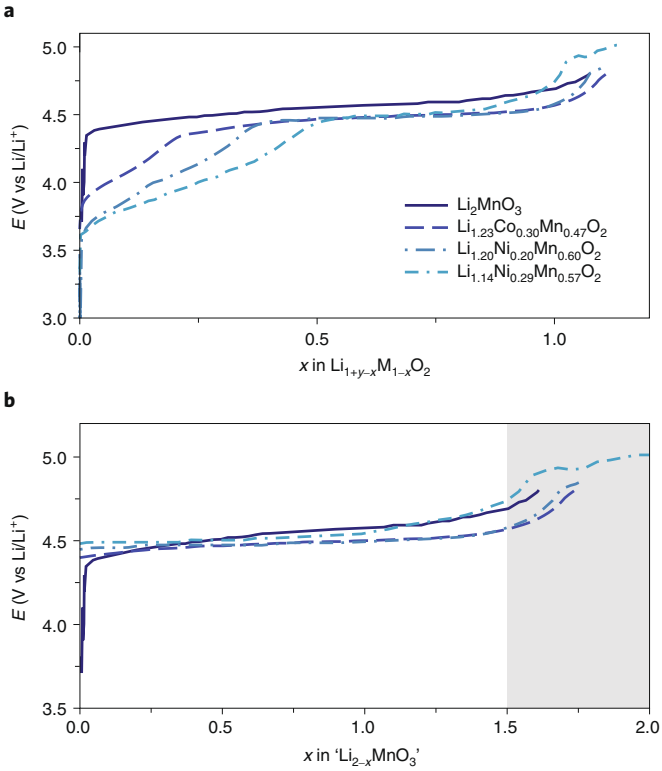

Fig. 1 | Comparison of the first-charge voltage curves of pure Li_2MnO_3 and Li_2MnO_3/$LiMO_2$ composites. a, The first-charge voltage curves for Li_2MnO_3/$LiMO_2$ composites. **b**, The portion of the first-charge voltage curves arising from the Li_2MnO_3 component of Li_2MnO_3/$LiMO_2$ composites. The shaded region in **b** highlights that the plateau ends when approximately 1.5 Li has been removed. Data for $Li_{1.20}Ni_{0.20}Mn_{0.60}O_2$, and $Li_{1.14}Ni_{0.29}Mn_{0.57}O_2$ from ref. [67]; data for $Li_{1.23}Co_{0.30}Mn_{0.47}O_2$ and Li_2MnO_3 from refs. [6,11], respectively.

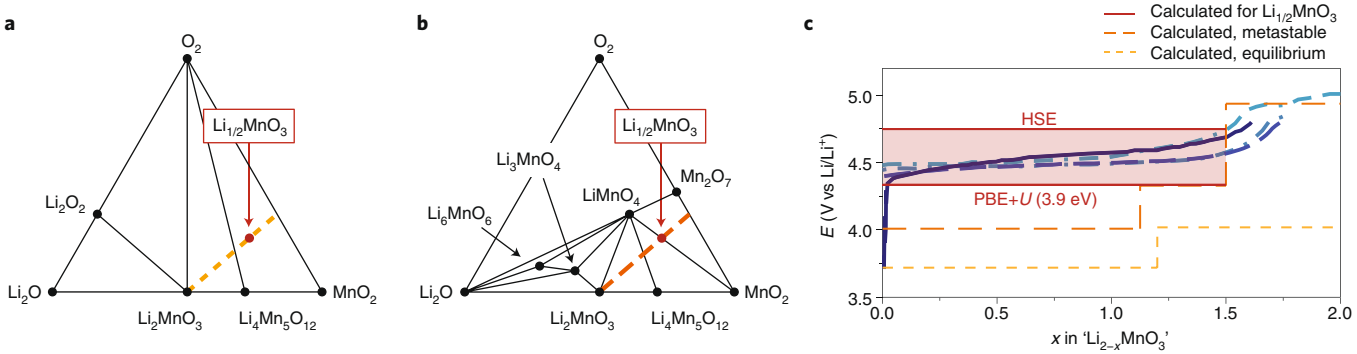

Fig. 2 | Theoretical phase diagrams and voltage curves for the Li_2O–MnO_2–O_2 system. a, The equilibrium Li_2O–MnO_2–O_2 phase diagram shows that the equilibrium delithiation mechanism (represented by the dashed line) involves the evolution of O_2 gas. **b**, The metastable phase diagram shows that if the formation of oxygen–oxygen bonds were kinetically impeded, then delithiation could occur via the oxidation of Mn to the +7 oxidation state in the form of $LiMnO_4$ and Mn_2O_7. In both **a** and **b**, the hypothesized $Li_{1/2}MnO_3$ phase, which is not a ground state in either phase diagram, is represented by a red dot. **c**, Comparison between the experimental voltage curves for Li_2MnO_3 and the Li_2MnO_3 component of composites[6,11,67], and the theoretical voltage curves for three mechanisms: the equilibrium pathway on the phase diagram in **a**, the equilibrium pathway on the metastable phase diagram shown in **b**, and the delithiation of Li_2MnO_3 to $Li_{1/2}MnO_3$. The experimental voltage curves are the same as those shown in Fig. 1b. The spread of predicted voltages for the Li_2MnO_3 to $Li_{1/2}MnO_3$ pathway using different first-principles approaches (that is, PBE+*U* and HSE) is shown as a red band.

Mn from a formal oxidation state of +4 to +7. The importance of this mechanism is revealed when we explore a scenario in which the dimerization of oxygen is kinetically limited. To this end, we consider the metastable phase diagram obtained by excluding all phases that exhibit covalent oxygen–oxygen bonds (that is, O_2, Li_2O_2, LiO_2 and LiO_3). Within this metastable phase diagram, the equilibrium reaction pathway (represented by the dashed line in Fig. 2b) occurs via the oxidation of Mn^{4+} to Mn^{7+} through a series of three-phase reactions that yield the Mn^{4+} compounds MnO_2 and $Li_4Mn_5O_{12}$ and the Mn^{7+} compounds $LiMnO_4$ and Mn_2O_7.

The observed voltage curves suggest that the system does not follow this sequence of reactions. Figure 2c compares the experimentally observed first-charge voltage curves for Li_2MnO_3 (ref. [11]) and the Li_2MnO_3 components of composite materials[6,67] with the

calculated voltage curves for the metastable reaction pathway (dashed orange line) and the true equilibrium pathway (dashed yellow line). The absence of a step at $x = 9/8$ in the observed voltage curves implies that the reaction does not proceed by the above three-phase reactions.

It would not be surprising for these three-phase reactions to be kinetically slow, as they require the long-range diffusion of Mn or O. For example, if the oxygen sublattice were to remain intact, Li extraction would need to be accompanied by a redistribution of Mn such that some regions become enriched in Mn and others become depleted. The sluggish mobility of Mn relative to that of Li makes this scenario unlikely, suggesting a kinetically simpler reaction that results in a metastable $Li_{2-x}MnO_3$ compound according to equation (3):

$$Li_2MnO_3 \rightarrow Li_{2-x}MnO_3 + xLi^+ + xe^- \quad (3)$$

The notion of a metastable $Li_{2-x}MnO_3$ phase forming on first charge is not new: the oxygen-redox hypothesis represents the formation of a metastable $Li_{2-x}MnO_3$ phase in which some of the oxygen anions are in the −1 oxidation state[25,29,37]. However, the fact that the equilibrium phases (within the metastable phase diagram of Fig. 2b) contain Mn^{4+} and Mn^{7+} suggests that the $Li_{2-x}MnO_3$ reaction product could be a mixed-valence Mn^{4+}/Mn^{7+} compound. This is further motivated by the fact that many of the Mn^{4+} and Mn^{7+} phases in the metastable phase diagram favour fcc oxygen sublattices[74–77] and therefore could form a solid solution or nanocomposite.

Critical analysis of Mn oxidation

To explore the possible formation of $Li_{2-x}MnO_3$ compounds containing Mn^{4+} and Mn^{7+}, we calculated from first principles the energies of $Li_{1/2}MnO_3$ structures that have an fcc oxygen sublattice. This composition (represented by a red circle in Fig. 2a and b) approximates the capacity at the end of the first-charge plateau and requires the oxidation of half of the Mn^{4+} ions to Mn^{7+}. Because Mn^{4+} prefers octahedral coordination[74] and Mn^{7+} prefers tetrahedral coordination[76], we considered structures wherein half of the Mn reside in tetrahedral sites and half in octahedral sites. The lowest-energy structure found is shown in Fig. 3a. (See Supplementary Information for additional details.)

The voltage for the reaction $Li_2MnO_3 \rightarrow Li_{1/2}MnO_3 + \frac{3}{2}Li^+ + \frac{3}{2}e^-$ calculated with the Perdew–Burke–Ernzerhof functional with on-site Coulomb corrections (PBE+*U*) is 4.34 V for $U = 3.9$ eV. (The predicted voltage is 4.55 V when $U = 5$ eV.) The hybrid Heyd–Scuseria–Ernzerhof (HSE) functional predicts a slightly higher voltage of 4.75 V. These values are consistent with the experimentally observed voltage, considering that the error in intercalation voltages for transition-metal oxides predicted by PBE+*U* and HSE is often several tenths of a volt[78]. Preliminary calculations (using PBE+*U*, HSE and strongly constrained and appropriately normed (SCAN) functionals; see Supplementary Information) also suggest that Mn oxidation is thermodynamically favoured over O^{2-}/O^- oxygen redox. However, as discussed in the Supplementary Information, a definitive determination of which mechanism is thermodynamically favoured will require more advanced approaches to electronic structure calculations.

The energy for a phase to decompose into its equilibrium state can serve as a rough guide to whether that phase can be produced in a laboratory[79]. The energy for the decomposition of $Li_{1/2}MnO_3$ into the metastable phases of Fig. 2b through the reaction $Li_{1/2}MnO_3 \rightarrow \frac{1}{2}LiMnO_4 + \frac{1}{2}MnO_2$ is −0.15 eV per atom. Further decomposition into the true equilibrium state through the reaction

$$\frac{1}{2}LiMnO_4 + \frac{1}{2}MnO_2 \rightarrow \frac{1}{8}Li_4Mn_5O_{12} + \frac{3}{8}MnO_2 + \frac{3}{8}O_2 \quad (4)$$

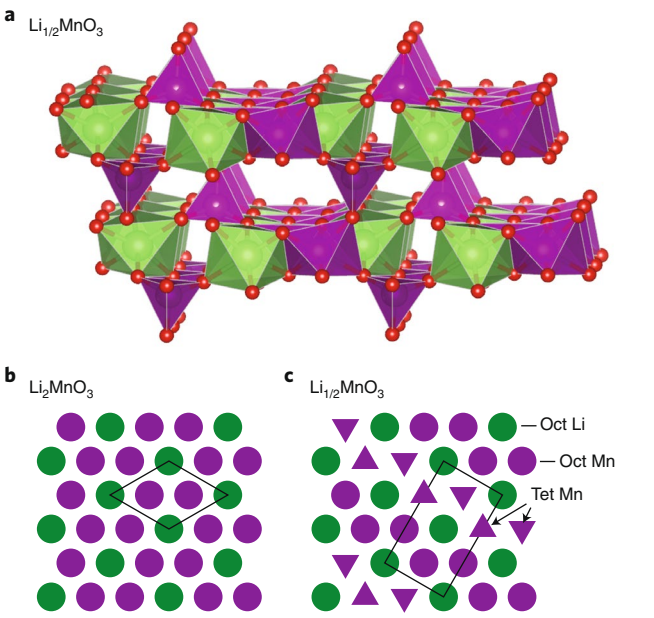

Fig. 3 | Hypothesized $Li_{1/2}MnO_3$ structure representing the Li_2MnO_3 component of the cathode material at the end of the activation plateau. **a**, Relaxed crystal structure for the hypothesized $Li_{1/2}MnO_3$ structure, with green, purple and red corresponding to Li, Mn and O, respectively. **b**,**c**, Comparison of the Li_2MnO_3 and hypothesized $Li_{1/2}MnO_3$ structures. The circles represent the octahedral (Oct) sites within the transition-metal layer. The triangles represent the tetrahedral (Tet) sites in the Li layer that reside directly above and below the octahedral sites in the transition-metal layer. The black lines denote the unit cell.

has an energy of −0.10 eV per atom. (Including the entropy of gas-phase O_2 under standard conditions[80] yields a reaction free energy of −0.15 eV per atom.) Given that these reaction energies are comparable to the decomposition energies of other metastable compounds that can be synthesized under laboratory conditions[79], it is plausible that $Li_{1/2}MnO_4$ could form during an electrochemical experiment.

The hypothesized $Li_{1/2}MnO_3$ structure is intended to be a representative model of the local structure of the charged Li_2MnO_3 component of Li-excess manganese oxides, and other $Li_{2-x}MnO_3$ configurations with similar local structure could also form upon charge before $Li_{1/2}MnO_3$. The presence of a non-negligible slope in the 4.5 V 'plateau' of Fig. 1b could be due to the formation of such configurations. A key property of the $Li_{1/2}MnO_3$ structure shown in Fig. 3a is that it provides each oxygen site with a local environment that is consistent with Pauling's second rule[81]. Structures with severe violations of Pauling's second rule were predicted to be significantly higher in energy.

Mixed-valence Mn^{4+}/Mn^{7+} phases similar to that of Fig. 3a are kinetically accessible from the original Li_2MnO_3 phase because their formation requires only a single octahedral to tetrahedral hop for each Mn that migrates. Figure 3b and c illustrates how Li_2MnO_3 could topotactically transform into $Li_{1/2}MnO_3$. Two-thirds (one-third) of the octahedral sites of the transition-metal layer of Li_2MnO_3 are occupied by Mn (Li), as shown in Fig. 3b. Figure 3c shows how the hypothesized $Li_{1/2}MnO_3$ structure can emerge if one-quarter of the Mn atoms migrate to tetrahedral sites in the Li layer above (upward-pointing triangles) and one-quarter to tetrahedral sites in the Li layer below (downward-pointing triangles).

If discharge proceeds via the reduction of Mn^{7+} to Mn^{4+}, then the availability of multiple tetrahedral to octahedral migration pathways can explain the absence of the 4.5 V plateau on subsequent

cycles: tetrahedral Mn ions are unlikely to return to their original octahedral sites during the first discharge. A tetrahedral Mn ion can migrate to any of the four octahedral sites with which it shares a face. (In the $Li_{1/2}MnO_3$ structure of Fig. 3a, one of these sites is likely to be inaccessible because it shares a face with another tetrahedral Mn ion.) After the first discharge, the cation ordering (within the Li_2MnO_3 component) is likely to resemble a disordered rocksalt more than layered Li_2MnO_3. The second-charge voltage curve will then differ from the first-charge voltage curve, with the diversity of local Mn environments yielding contributions to the capacity across a wide voltage range. Voltage fade upon further cycling[7] could arise from further rearrangement of Mn ions.

The migration of Mn between tetrahedral and octahedral sites can also explain the large hysteresis in the voltage curve[6,82,83]. If the kinetics of Mn migration between octahedral and tetrahedral sites is rate-limiting, then discharge could proceed via the reduction of Mn^{7+} to Mn^{5+}, which would not require the migration of manganese ions because Mn^{5+} favours tetrahedral coordination[84]. The difference in voltage between the Mn^{4+}/Mn^{7+} and Mn^{5+}/Mn^{7+} redox couples would manifest as a polarization in the voltage curve, and energy would be lost in the form of heat released by the gradual migration of manganese ions to octahedral sites. (The reduction of octahedral Mn^{4+} remaining at the end of charge to Mn^{3+} could similarly occur without Mn migration.) Such a process is analogous to how sluggish diffusion can lead to hysteresis in conversion electrodes[83].

The notion that octahedral/tetrahedral migration is responsible for the unusual electrochemical behaviour of the Li-excess manganese oxides is supported by similar behaviour in $LiCrO_2 \cdot Li_2MnO_3$ composites. In these materials, (de)intercalation below 4.4 V operates on the Cr^{3+}/Cr^{6+} redox couple and is accompanied by the migration of Cr between octahedral and tetrahedral sites[85–87]. The voltage profile of these composites changes markedly after the first charge, and this 'activation' phenomenon has been attributed to the migration of Cr ions to octahedral sites in the Li layer during the first discharge[87]. During subsequent cycling, $LiCrO_2 \cdot Li_2MnO_3$ composites also exhibit considerable polarization (~0.3 V)[85]. Similar activation and hysteresis have also been observed in $LiCrO_2 \cdot Li_2TiO_3$ composites[88].

If reversible Mn^{4+}/Mn^{7+} redox were responsible for the anomalous capacity of Li-excess manganese oxides, then experimental verification would be challenging because of the fragility of oxides containing Mn^{7+}. For example, beam damage can reduce Mn^{7+} to Mn^{4+} in $KMnO_4$ during Mn K- and L-edge X-ray absorption experiments[89,90], as well as in Mn L-edge electron energy-loss spectroscopy[91]. Experiments have also found $KMnO_4$ to decompose during O K-edge X-ray absorption measurements[92]. (Although studies on Mn^{7+} compounds such as $KMnO_4$ can provide a useful guide as to the fragility of a Mn^{7+}-containing cathode, a charged Li-excess cathode could potentially be degraded more rapidly than reference compounds owing to differences in bonding, particle size and microstructure.) The spectroscopic observation of Mn^{4+} in charged cathodes therefore does not definitively rule out the presence of Mn^{7+}. Experiments showing that beam damage can induce a RIXS feature in $LiAlO_2$ that is identical to the feature observed in charged Li-excess cathodes[42] support this scenario, as does the observation[40] of a similar RIXS feature in Li_2O. Lastly, we note that in situ beam damage may not greatly affect electrochemical performance because in typical experiments, the beam covers only a small fraction of the electrode area.

Despite the fragility of Mn^{7+} compounds, there is experimental evidence to suggest the presence of Mn^{7+} at the end of charge. First, although the small size of the pre-edge peak in the Mn K-edge indicates that most of the signal originates from octahedral Mn, changes in the Mn K-edge measured in situ are consistent with the formation of a small amount of Mn^{7+}. These changes include a shift

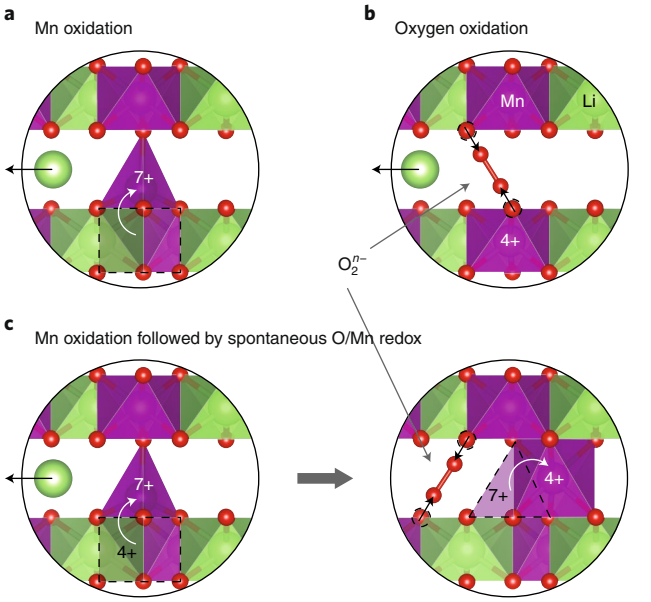

Fig. 4 | Alternative charge mechanisms in Li-excess manganese oxides. **a**, The oxidation of Mn^{4+} to Mn^{7+}. **b**, The oxidation of oxygen ions to form peroxide ions or internally trapped oxygen molecules. **c**, The oxidation of Mn^{4+} to Mn^{7+} followed by the spontaneous formation of peroxide ions or trapped oxygen molecules and the reduction of Mn. Colours as in Fig. 3.

of the main peak to higher energy and a growth of the pre-edge peak[11,26,28,30]. Second, a recent in situ diffraction study on a Li-excess cathode concluded that transition-metal ions migrate to tetrahedral sites in the Li layer during charge and return to octahedral sites on discharge[93]. Lastly, the Raman feature attributed to the reversible formation of peroxide ions is also consistent with tetrahedral Mn^{7+} (refs. [45,94]).

Figure 4a, b illustrates the two alternatives to the lattice oxygen redox hypothesis that we have explored so far. Although the formation of Mn^{7+} (Fig. 4a) as a charge mechanism is quite distinct from the formation of internally trapped O_2 molecules or peroxide ions (Fig. 4b), the two mechanisms could be linked. The migration of Mn to tetrahedral sites could trigger the spontaneous formation of O_2 molecules or peroxide ions, in which case the Mn^{7+} ions would be reduced and likely to return to octahedral sites, as shown in Fig. 4c. This scenario is consistent with spectroscopic observations showing Mn mainly in the +4 oxidation state and also can explain the activation process and hysteresis. The disappearance of the activation plateau after the first cycle could arise from the availability of multiple tetrahedral to octahedral migration pathways as discussed above, and the spontaneous formation of oxygen dimers could lead to hysteresis because charge and discharge would follow different reaction pathways: whereas charge would occur through the oxidation of Mn^{4+} to Mn^{7+} (as shown in Fig. 4c), discharge would occur through the reduction of O_2 or O_2^{2-} to O^{2-}.

In the case of pure Li_2MnO_3, the observation through DEMS of considerable O_2 release during the first charge and poor electrochemical reversibility[11] are consistent with the spontaneous decomposition of a Mn^{7+} phase. Other kinetic processes leading to oxygen evolution, such as the densification mechanism discussed above, may also occur. However, the agreement between the first-charge voltage curves (when appropriately normalized) of Li_2MnO_3 and of composite materials suggests that the electrochemical process occurring in these compounds is the same. Therefore, the embedding of Li_2MnO_3 in a nanocomposite may play an important role in stabilizing the Mn^{7+} phase formed on charge or stabilizing a structure containing peroxide ions or trapped oxygen molecules.

Conclusions

The experimental evidence for O^{2-}/O^{-} lattice oxygen redox in Li-excess materials is not yet conclusive, and alternative mechanisms require renewed attention. (We emphasize that although available experimental observations do not provide compelling direct evidence for O^{2-}/O^{-} redox, they also do not definitively rule it out.) We have highlighted several mechanisms that appear to be consistent with available data (illustrated in Fig. 4): the oxidation of Mn^{4+} to Mn^{7+} accompanied by a migration from octahedral to tetrahedral sites; the formation of peroxide ions or trapped molecular oxygen; and the formation of Mn^{7+} followed by the spontaneous dimerization of oxygen. We have explored in depth the oxidation of Mn^{4+} to Mn^{7+} and found this hypothesis to be compatible with experimental and first-principles thermodynamics, supported by the observation of tetrahedral occupancy at the end of charge through X-ray diffraction[93] and consistent with the electrochemical behaviour in Cr-based cathode materials which are known to undergo tetrahedral/octahedral migration[85–88]. The anomalous capacity may, however, involve contributions from multiple redox mechanisms. Furthermore, the redox mechanism on charge may be different from that on discharge (for example, the oxidation of Mn on charge and reduction of peroxide ions or trapped oxygen molecules on discharge). Advances in both experimental and theoretical methods could lead to a clearer understanding of the roles played by different mechanisms. Innovations in in situ experimental probes may be especially valuable because the excess capacity originates at high states of charge, where almost all intercalation compounds are metastable and highly susceptible to decomposition reactions. Techniques to probe for peroxide ions or molecular oxygen deep within cathode particles could also provide great insight.

Although our analysis focused on the Li-excess manganese oxides, the mechanisms discussed above could explain the anomalous capacity of certain manganese oxides used as electrodes in Na-ion batteries[15–18,95]. These materials behave similarly to the Li-excess manganese oxides in that they exhibit an anomalous capacity and significant polarization. However, they differ in that there is no apparent 'activation': the charge curve does not qualitatively change after the first cycle. This could arise from the large size of the Na^{+} ions relative to Mn^{4+} ions, which makes it unfavourable for Na^{+} and Mn^{4+} ions to reside in the same layer. This scenario is supported by recent experiments on a Zn-doped Na manganese oxide[18]: transmission electron microscopy indicated that cations migrated from the transition-metal layer to the Na layer during charge and returned to the transition-metal layer on discharge.

These mechanisms could also explain the behaviour of certain $4d/5d$ transition-metal oxides[19–24]. The electrochemical activity of these materials has been attributed to a combination of the oxidation of octahedral Ir/Ru ions and oxygen redox involving the formation of a peroxo-like $(O_2)^{n-}$ species or a true peroxide O_2^{2-} (refs. [20,23,24,31,53,96,97]). The electrochemical behaviour of these materials is nevertheless also consistent with the migration of oxidized Ir and Ru ions between octahedral and tetrahedral sites, as discussed in the Supplementary Information. A RIXS feature similar to that observed in Li-excess manganese oxides has also been observed in charged $Li_2Ir_{1/2}Sn_{1/2}O_3$ and could represent the decomposition products of a compound containing highly oxidized Ir (ref. [20]). Additionally, Raman signals associated with the anomalous capacity of Na_3RuO_4 and attributed to peroxide ions are also consistent with tetrahedral Ru^{7+} (refs. [97,98]).

If the Mn-oxidation mechanism is correct, it suggests a guiding principle for the design of high-capacity cathode materials: the use of a nanocomposite or alloy may allow one to access high oxidation states that otherwise would lead to the decomposition of the material. A challenge with such an approach is to manage the migration of transition-metal ions, as large changes in oxidation state are often accompanied by a change in coordination preferences. It may be possible to design cathode materials that use high oxidation states without inducing transition-metal migration or to design materials in which the migration of transition-metal ions is sufficiently facile and reversible to yield satisfactory electrochemical performance.

Methods

Density functional theory calculations were performed with the Vienna ab initio Simulation Package (VASP)[99–102] with projector augmented-wave (PAW) pseudopotentials[103]. All calculations were spin-polarized and used plane-wave basis sets with 530 eV energy cut-offs. PBE+U calculations[104] on oxides sampled the Brillouin zone with a k-point mesh density of at least 26 Å. HSE calculations[105,106] on oxides used a coarser density of at least 10 Å. Calculations on the primitive cell of bcc Li used a denser k-point mesh of $10 \times 10 \times 10$. The PBE+U calculations used the on-site Coulomb correction of ref. [107] for Mn d states with $U_{\mathrm{eff}} = 3.9$ eV and 5 eV. HSE calculations used the standard mixing parameter α of 0.25. Relaxations used Gaussian smearing of width 0.2 eV and were converged to within a force convergence criterion of 0.02 eV $Å^{-1}$ for both PBE+U and HSE calculations; these were followed by single-point calculations using the tetrahedron method with Blöchl corrections[108] to obtain accurate energies. Because magnetic studies show that interactions between edge-sharing Mn^{4+} ions are ferromagnetic[109], our calculations were restricted to ferromagnetic spin orderings.

Data availability

The analysis presented here can be reproduced with the data provided in the paper, supporting information and cited references. Additional calculation data generated during this study are available upon reasonable request.

Received: 24 July 2018; Accepted: 18 June 2019;
Published online: 29 July 2019

References

1. Lu, Z., Beaulieu, L. Y., Donaberger, R. A., Thomas, C. L. & Dahn, J. R. Synthesis, structure, and electrochemical behavior of $Li[Ni_xLi_{1/3-2x/3}Mn_{2/3-x/3}]O_2$. *J. Electrochem. Soc.* **149**, A778–A791 (2002).
2. Johnson, C. S. et al. The significance of the Li_2MnO_3 component in 'composite' $xLi_2MnO_3 \cdot (1-x)LiMn_{0.5}Ni_{0.5}O_2$ electrodes. *Electrochem. Commun.* **6**, 1085–1091 (2004).
3. Hong, J., Gwon, H., Jung, S.-K., Ku, K. & Kang, K. Review: Lithium-excess layered cathodes for lithium rechargeable batteries. *J. Electrochem. Soc.* **162**, A2447–A2467 (2015).
4. Hy, S. et al. Performance and design considerations for the lithium excess layered oxide positive electrode materials for lithium ion batteries. *Energy Environ. Sci.* **9**, 1931–1954 (2016).
5. Radin, M. D. et al. Narrowing the gap between theoretical and practical capacities in Li-ion layered oxide cathode materials. *Adv. Energy Mater.* **7**, 1602888 (2017).
6. Wei, Y. J. et al. Electrochemical kinetics and cycling performance of nano $Li[Li_{0.23}Co_{0.3}Mn_{0.47}]O_2$ cathode material for lithium ion batteries. *Electrochem. Commun.* **11**, 2008–2011 (2009).
7. Johnson, C. S., Li, N., Lefief, C., Vaughey, J. T. & Thackeray, M. M. Synthesis, characterization and electrochemistry of lithium battery electrodes: $xLi_2MnO_3 \cdot (1-x)LiMn_{0.333}Ni_{0.333}Co_{0.333}O_2$ $(0 \le x \le 0.7)$. *Chem. Mater.* **20**, 6095–6106 (2008).
8. Bettge, M. et al. Voltage fade of layered oxides: its measurement and impact on energy density. *J. Electrochem. Soc.* **160**, A2046–A2055 (2013).
9. Kalyani, P., Chitra, S., Mohan, T. & Gopukumar, S. Lithium metal rechargeable cells using Li_2MnO_3 as the positive electrode. *J. Power Sources* **80**, 103–106 (1999).
10. Robertson, A. D. & Bruce, P. G. Mechanism of electrochemical activity in Li_2MnO_3. *Chem. Mater.* **15**, 1984–1992 (2003).
11. Yu, D. Y. W., Yanagida, K., Kato, Y. & Nakamura, H. Electrochemical activities in Li_2MnO_3. *J. Electrochem. Soc.* **156**, A417–A424 (2009).
12. Park, Y. J. et al. Synthesis and electrochemical characteristics of $Li[Co_xLi_{(1/3-x/3)}Mn_{(2/3-2x/3)}]O_2$ compounds. *J. Electrochem. Soc.* **151**, A720–A727 (2004).
13. Yabuuchi, N. et al. High-capacity electrode materials for rechargeable lithium batteries: Li_3NbO_4-based system with cation-disordered rocksalt structure. *Proc. Natl Acad. Sci. USA* **112**, 7650–7655 (2015).
14. Yabuuchi, N. et al. Origin of stabilization and destabilization in solid-state redox reaction of oxide ions for lithium-ion batteries. *Nat. Commun.* **7**, 13814 (2016).
15. Yabuuchi, N. et al. A new electrode material for rechargeable sodium batteries: P2-type $Na_{2/3}[Mg_{0.28}Mn_{0.72}]O_2$ with anomalously high reversible capacity. *J. Mater. Chem. A* **2**, 16851–16855 (2014).
16. Maitra, U. et al. Oxygen redox chemistry without excess alkali-metal ions in $Na_{2/3}[Mg_{0.28}Mn_{0.72}]O_2$. *Nat. Chem.* **10**, 288–295 (2018).

17. Mortemard de Boisse, B. et al. Highly reversible oxygen-redox chemistry at 4.1 V in $Na_{4/7-x}[\Upsilon_{1/7}Mn_{6/7}]O_2$ (Υ: Mn vacancy). *Adv. Energy Mater.* **2**, 1800409 (2018).
18. Bai, X. et al. Anionic redox activity in a newly Zn-doped sodium layered oxide P2-$Na_{2/3}Mn_{1-y}Zn_yO_2$ ($0 < y < 0.23$). *Adv. Energy Mater.* **8**, 1802379 (2018).
19. Sathiya, M. et al. Reversible anionic redox chemistry in high-capacity layered-oxide electrodes. *Nat. Mater.* **12**, 827–835 (2013).
20. Hong, J. et al. Metal–oxygen decoordination stabilizes anion redox in Li-rich oxides. *Nat. Mater.* **18**, 256–265 (2019).
21. Pearce, P. E. et al. Evidence for anionic redox activity in a tridimensional-ordered Li-rich positive electrode β-Li_2IrO_3. *Nat. Mater.* **16**, 580–586 (2017).
22. McCalla, E. et al. Visualization of O–O peroxo-like dimers in high-capacity layered oxides for Li-ion batteries. *Science* **350**, 1516–1521 (2015).
23. Saubanère, M., McCalla, E., Tarascon, J.-M. & Doublet, M.-L. The intriguing question of anionic redox in high-energy density cathodes for Li-ion batteries. *Energy Environ. Sci.* **9**, 984–991 (2016).
24. Assat, G. & Tarascon, J.-M. Fundamental understanding and practical challenges of anionic redox activity in Li-ion batteries. *Nat. Energy* **3**, 373–386 (2018).
25. Seo, D. et al. The electronic origin of the oxygen redox activity in Li-excess cathode materials. *Nat. Chem.* **8**, 692–697 (2016).
26. Luo, K. et al. Charge-compensation in 3 *d*-transition-metal-oxide intercalation cathodes through the generation of localized electron holes on oxygen. *Nat. Chem.* **8**, 684–691 (2016).
27. Koga, H. et al. Different oxygen redox participation for bulk and surface: a possible global explanation for the cycling mechanism of $Li_{1.20}Mn_{0.54}Co_{0.13}Ni_{0.13}O_2$. *J. Power Sources* **236**, 250–258 (2013).
28. Koga, H. et al. Operando X-ray absorption study of the redox processes involved upon cycling of the Li-rich layered oxide $Li_{1.20}Mn_{0.54}Co_{0.13}Ni_{0.13}O_2$ in Li ion batteries. *J. Phys. Chem. C.* **118**, 5700–5709 (2014).
29. Koyama, Y., Tanaka, I., Nagao, M. & Kanno, R. First-principles study on lithium removal from Li_2MnO_3. *J. Power Sources* **189**, 798–801 (2009).
30. Gent, W. E. et al. Coupling between oxygen redox and cation migration explains unusual electrochemistry in lithium-rich layered oxides. *Nat. Commun.* **8**, 2091 (2017).
31. Xu, J. et al. Elucidating anionic oxygen activity in lithium-rich layered oxides. *Nat. Commun.* **9**, 947 (2018).
32. Kubobuchi, K. et al. Mn $L_{2,3}$-edge X-ray absorption spectroscopic studies on charge–discharge mechanism of Li_2MnO_3. *Appl. Phys. Lett.* **104**, 053906 (2014).
33. Rana, J. et al. Structural changes in Li_2MnO_3 cathode material for Li-ion batteries. *Adv. Energy Mater.* **4**, 1300998 (2014).
34. Oishi, M. et al. Direct observation of reversible charge compensation by oxygen ion in Li-rich manganese layered oxide positive electrode material, $Li_{1.16}Ni_{0.15}Co_{0.19}Mn_{0.50}O_2$. *J. Power Sources* **276**, 89–94 (2015).
35. Tran, N. et al. Mechanisms associated with the 'plateau' observed at high voltage for the overlithiated $Li_{1.12}Ni_{0.425}Mn_{0.425}Co_{0.15})_{0.88}O_2$ system. *Chem. Mater.* **20**, 4815–4825 (2008).
36. Armstrong, A. R. et al. Demonstrating oxygen loss and associated structural reorganization in the lithium battery cathode $Li[Ni_{0.2}Li_{0.2}Mn_{0.6}]O_2$. *J. Am. Chem. Soc.* **128**, 8694–8698 (2006).
37. Lee, E. & Persson, K. A. Structural and chemical evolution of the layered Li-excess Li_xMnO_3 as a function of Li content from first-principles calculations. *Adv. Energy Mater.* **4**, 1400498 (2014).
38. Malik, R., Abdellahi, A. & Ceder, G. A Critical review of the Li insertion mechanisms in $LiFePO_4$ electrodes. *J. Electrochem. Soc.* **160**, A3179–A3197 (2013).
39. Rinaldo, S. G. et al. Physical theory of voltage fade in lithium- and manganese-rich transition metal oxides. *J. Electrochem. Soc.* **162**, A897–A904 (2015).
40. Zhuo, Z. et al. Spectroscopic signature of oxidized oxygen states in peroxides. *J. Phys. Chem. Lett.* **9**, 6378–6384 (2018).
41. Glans, P. et al. Resonant X-ray emission spectroscopy of molecular oxygen. *Phys. Rev. Lett.* **76**, 2448–2451 (1996).
42. Lebens-Higgins, Z. W. et al. Distinction between intrinsic and X-ray induced oxidized oxygen states in Li-rich 3 *d* layered oxides and $LiAlO_2$. *J. Phys. Chem. C* **123**, 13201–13207 (2019).
43. Bercx, M., Slap, L., Partoens, B. & Lamoen, D. First-principles investigation of the stability of the oxygen framework of Li-rich battery cathodes. *MRS Adv.* **4**, 813–820 (2017).
44. Chen, H. & Islam, M. S. Lithium extraction mechanism in Li-rich Li_2MnO_3 involving oxygen hole formation and dimerization. *Chem. Mater.* **28**, 6656–6663 (2016).
45. Li, X. et al. Direct visualization of the reversible O^{2-}/O^- redox process in Li-rich cathode materials. *Adv. Mater.* **30**, 1705197 (2018).
46. Van der Ven, A., Aydinol, M. K., Ceder, G., Kresse, G. & Hafner, J. First-principles investigation of phase stability in Li_xCoO_2. *Phys. Rev. B* **58**, 2975–2987 (1998).
47. Wolverton, C. & Zunger, A. First-principles prediction of vacancy order–disorder and intercalation battery voltages in Li_xCoO_2. *Phys. Rev. Lett.* **81**, 606–609 (1998).
48. Qiu, B., Zhang, M., Xia, Y., Liu, Z. & Meng, Y. S. Understanding and controlling anionic electrochemical activity in high-capacity oxides for next generation Li-ion batteries. *Chem. Mater.* **29**, 908–915 (2017).
49. Okubo, M. & Yamada, A. Molecular orbital principles of oxygen-redox battery electrodes. *ACS Appl. Mater. Interfaces* **9**, 36463–36472 (2017).
50. Li, B. & Xia, D. Anionic redox in rechargeable lithium batteries. *Adv. Mater.* **29**, 1701054 (2017).
51. Schirmer, O. F. Smoky coloration of quartz caused by bound small hole polaron optical absorption. *Solid State Commun.* **18**, 1349–1351 (1976).
52. Griscom, D. L. Self-trapped holes in pure-silica glass: a history of their discovery and characterization and an example of their critical significance to industry. *J. Non Cryst. Solids* **352**, 2601–2617 (2006).
53. Grimaud, A., Hong, W. T., Shao-Horn, Y. & Tarascon, J.-M. Anionic redox processes for electrochemical devices. *Nat. Mater.* **15**, 121–126 (2016).
54. Lee, P. A., Nagaosa, N. & Wen, X. G. Doping a Mott insulator: physics of high-temperature superconductivity. *Rev. Mod. Phys.* **78**, 17–85 (2006).
55. Subedi, A., Peil, O. E. & Georges, A. Low-energy description of the metal–insulator transition in the rare-earth nickelates. *Phys. Rev. B* **91**, 075128 (2015).
56. Hu, E. et al. Evolution of redox couples in Li- and Mn-rich cathode materials and mitigation of voltage fade by reducing oxygen release. *Nat. Energy* **3**, 690–698 (2018).
57. Yang, W. & Devereaux, T. P. Anionic and cationic redox and interfaces in batteries: advances from soft X-ray absorption spectroscopy to resonant inelastic scattering. *J. Power Sources* **389**, 188–197 (2018).
58. Dai, K. et al. High reversibility of lattice oxygen redox in Na-ion and Li-ion batteries quantified by direct bulk probes of both anionic and cationic redox reactions. *Joule* **3**, 518–541 (2019).
59. Chan, M. K. Y. et al. Structure of lithium peroxide. *J. Phys. Chem. Lett.* **2**, 2483–2486 (2011).
60. Wang, L., Maxisch, T. & Ceder, G. A first-principles approach to studying the thermal stability of oxide cathode materials. *Chem. Mater.* **19**, 543–552 (2007).
61. Yabuuchi, N., Yoshii, K., Myung, S. T., Nakai, I. & Komaba, S. Detailed studies of a high-capacity electrode material for rechargeable batteries, Li_2MnO_3–$LiCo_{1/3}Ni_{1/3}Mn_{1/3}O_2$. *J. Am. Chem. Soc.* **133**, 4404–4419 (2011).
62. Lu, Z. & Dahn, J. R. Understanding the anomalous capacity of Li/$Li[Ni_xLi_{(1/3-2x/3)}Mn_{(2/3-x/3)}]O_2$ cells using in situ X-ray diffraction and electrochemical studies. *J. Electrochem. Soc.* **149**, A815–A822 (2002).
63. Pasero, D., McLaren, V., De Souza, S. & West, A. R. Oxygen nonstoichiometry in Li_2MnO_3: an alternative explanation for its anomalous electrochemical activity. *Chem. Mater.* **17**, 345–348 (2005).
64. Kubota, K. et al. Direct synthesis of oxygen-deficient Li_2MnO_{3-x} for high capacity lithium battery electrodes. *J. Power Sources* **216**, 249–255 (2012).
65. Okamoto, Y. Ambivalent effect of oxygen vacancies on Li_2MnO_3: a first-principles study. *J. Electrochem. Soc.* **159**, A152–A157 (2012).
66. Armstrong, A. R., Robertson, A. D. & Bruce, P. G. Overcharging manganese oxides: extracting lithium beyond Mn^{4+}. *J. Power Sources* **146**, 275–280 (2005).
67. Ohzuku, T., Nagayama, M., Tsuji, K. & Ariyoshi, K. High-capacity lithium insertion materials of lithium nickel manganese oxides for advanced lithium-ion batteries: toward rechargeable capacity more than 300 mA h g^{-1}. *J. Mater. Chem.* **21**, 10179 (2011).
68. Jain, A. et al. Commentary. The materials project: a materials genome approach to accelerating materials innovation. *APL Mater.* **1**, 011002 (2013).
69. Ong, S. P., Wang, L., Kang, B. & Ceder, G. Li–Fe–P–O_2 phase diagram from first principles calculations. *Chem. Mater.* **77**, 1798–1807 (2008).
70. Jain, A. et al. Formation enthalpies by mixing GGA and GGA + U calculations. *Phys. Rev. B* **84**, 045115 (2011).
71. Strehle, B. et al. The role of oxygen release from Li- and Mn-rich layered oxides during the first cycles investigated by on-line electrochemical mass spectrometry. *J. Electrochem. Soc.* **164**, A400–A406 (2017).
72. Thackeray, M. M., Chan, M. K. Y., Trahey, L., Kirklin, S. & Wolverton, C. Vision for designing high-energy, hybrid Li ion/Li–O_2 cells. *J. Phys. Chem. Lett.* **4**, 3607–3611 (2013).
73. Ruther, R. E., Callender, A. F., Zhou, H., Martha, S. K. & Nanda, J. Raman microscopy of lithium-manganese-rich transition metal oxide cathodes. *J. Electrochem. Soc.* **162**, A98–A102 (2014).
74. Thackeray, M. M. Manganese oxides for lithium batteries. *Prog. Solid State Chem.* **25**, 1–71 (1997).
75. Jansen, V. M. & Hoppe, R. Zur Kenntnis der NaCl-Strukturfamilie: Neue Untersuchungen an Li_2MnO_3. *Z. Anorg. Allg. Chem.* **397**, 279–289 (1973).
76. Fischer, D., Hoppe, R., Schäfer, W. & Knight, K. S. Koordinationszahl 4 oder 6 für Lithium? Die Kristallstruktur von wasserfreiem Lithiumpermanganat, $Li[MnO_4]$. *Z. Anorg. Allg. Chem.* **619**, 1419–1425 (1993).

77. Kitchaev, D. A. et al. Energetics of MnO_2 polymorphs in density functional theory. *Phys. Rev. B* **93**, 045132 (2016).
78. Chevrier, V. L., Ong, S. P., Armiento, R., Chan, M. K. Y. & Ceder, G. Hybrid density functional calculations of redox potentials and formation energies of transition metal compounds. *Phys. Rev. B* **82**, 075122 (2010).
79. Aykol, M., Dwaraknath, S. S., Sun, W. & Persson, K. A. Thermodynamic limit for synthesis of metastable inorganic materials. *Sci. Adv.* **4**, eaaq0148 (2018).
80. Chase, M. W. Jr. *NIST-JANAF Thermochemical Tables* (American Chemical Society, 1998).
81. Pauling, L. *The Nature of the Chemical Bond and the Structure of Molecules and Crystals: An Introduction to Modern Structural Chemistry* (Cornell Univ. Press, 1960).
82. Zheng, J. et al. Electrochemical kinetics and performance of layered composite cathode material $Li[Li_{0.2}Ni_{0.2}Mn_{0.6}]O_2$. *J. Electrochem. Soc.* **160**, 2212–2219 (2013).
83. Yu, H.-C. et al. Designing the next generation high capacity battery electrodes. *Energy Environ. Sci.* **7**, 1760–1768 (2014).
84. Li, V. Von & Hoppe, V. G. M. R. Zum thermischen Verhalten von Li_3MnO_4 I. 1. Über α- und β-Li_3MnO_4. **266**, 249–256 (1976).
85. Ammundsen, B. et al. Local structure and first cycle redox mechanism of layered $Li_{1.2}Cr_{0.4}Mn_{0.4}O_2$ cathode material. *J. Electrochem. Soc.* **149**, A431–A436 (2002).
86. Balasubramanian, M., McBreen, J., Davidson, I. J., Whitfield, P. S. & Kargina, I. In situ X-ray absorption study of a layered manganese-chromium oxide-based cathode material. *J. Electrochem. Soc.* **149**, A176–A184 (2002).
87. Lu, Z. & Dahn, J. R. In situ and ex situ XRD investigation of $Li[Cr_xLi_{1/3-x/3}Mn_{2/3-2x/3}]O_2$ ($x = 1/3$) cathode material. *J. Electrochem. Soc.* **150**, A1044–A1051 (2003).
88. Na, Y., Ho, S., Chan, Y. & Bin, S. Characteristics of Li_2TiO_3–$LiCrO_2$ composite cathode powders prepared by ultrasonic spray pyrolysis. *J. Power Sources* **244**, 336–343 (2013).
89. Chalmin, E., Farges, F. & Brown, G. E. A pre-edge analysis of Mn K-edge XANES spectra to help determine the speciation of manganese in minerals and glasses. *Contrib. Mineral. Petrol.* **157**, 111–126 (2009).
90. Van Schooneveld, M. M. & DeBeer, S. A close look at dose: toward L-edge XAS spectral uniformity, dose quantification and prediction of metal ion photoreduction. *J. Electron Spectrosc.* **198**, 31–56 (2015).
91. Garvie, L. A. J. & Craven, A. J. High-resolution parallel electron energy-loss spectroscopy of Mn $L_{2,3}$-edges in inorganic manganese compounds. *Phys. Chem. Miner.* **21**, 191–206 (1994).
92. Minasian, S. G. et al. Covalency in metal–oxygen multiple bonds evaluated using oxygen K-edge spectroscopy and electronic structure theory. *J. Am. Chem. Soc.* **135**, 1864–1871 (2013).
93. Kleiner, K. et al. Origin of high capacity and poor cycling stability of Li-rich layered oxides — a long-duration in situ synchrotron powder diffraction study. *Chem. Mater.* **30**, 3656–3667 (2018).
94. Kiefer, W. & Bernstein, H. J. Rotating Raman sample technique for colored crystal powders; resonance Raman effect in solid $KMnO_4$. *Appl. Spectrosc.* **25**, 609–613 (1971).
95. Du, K. et al. Exploring reversible oxidation of oxygen in a manganese oxide. *Energy Environ. Sci.* **9**, 2575–2577 (2016).
96. Ben Yahia, M., Vergnet, J., Saubanère, M. & Doublet, M. L. Unified picture of anionic redox in Li/Na-ion batteries. *Nat. Mater.* **18**, 496–502 (2019).
97. Qiao, Y. et al. Reversible anionic redox activity in Na_3RuO_4 cathodes: a prototype Na-rich layered oxide. *Energy Environ. Sci.* **11**, 299–305 (2018).
98. Griffith, W. P. Infrared spectra of tetrahedral oxyanions of the transition metals. *J. Chem. Soc. A* 1467–1468 (1966).
99. Kresse, G. & Hafner, J. Ab initio molecular dynamics for liquid metals. *Phys. Rev. B* **47**, 558–561 (1993).
100. Kresse, G. & Hafner, J. Ab initio molecular-dynamics simulation of the liquid-metal–amorphous-semiconductor transition in germanium. *Phys. Rev. B* **49**, 14251–14269 (1994).
101. Kresse, G. & Furthmüller, J. Efficiency of ab-initio total energy calculations for metals and semiconductors using a plane-wave basis set. *Comput. Mater. Sci.* **6**, 15–50 (1996).
102. Kresse, G. & Furthmüller, J. Efficient iterative schemes for ab initio total-energy calculations using a plane-wave basis set. *Phys. Rev. B* **54**, 11169–11186 (1996).
103. Blöchl, P. E. Projector augmented-wave method. *Phys. Rev. B* **50**, 17953–17979 (1994).
104. Perdew, J. P., Burke, K. & Ernzerhof, M. Generalized gradient approximation made simple. *Phys. Rev. Lett.* **77**, 3865–3868 (1996).
105. Heyd, J., Scuseria, G. E. & Ernzerhof, M. Hybrid functionals based on a screened Coulomb potential. *J. Chem. Phys.* **118**, 8207–8215 (2003).
106. Krukau, A. V., Vydrov, O. A., Izmaylov, A. F. & Scuseria, G. E. Influence of the exchange screening parameter on the performance of screened hybrid functionals. *J. Chem. Phys.* **125**, 224106 (2006).
107. Dudarev, S., Botton, G., Savrasov, S., Humphreys, C. & Sutton, A. Electron-energy-loss spectra and the structural stability of nickel oxide: an LSDA+*U* study. *Phys. Rev. B* **57**, 1505–1509 (1998).
108. Blöchl, P., Jepsen, O. & Andersen, O. Improved tetrahedron method for Brillouin-zone integrations. *Phys. Rev. B* **49**, 16223–16233 (1994).
109. Chernova, N. A. et al. What can we learn about battery materials from their magnetic properties? *J. Mater. Chem.* **21**, 9865–9875 (2011).

Acknowledgements

We thank L. Piper and Z. Lebens-Higgins for the insightful discussion. This work was supported as part of the NorthEast Center for Chemical Energy Storage (NECCES), an Energy Frontier Research Center funded by the US Department of Energy, Office of Science, Basic Energy Sciences under award no. DE- SC0012583. The contributions of R.S. were supported as part of the Center for Synthetic Control Across Length-scales for Advancing Rechargeables (SCALAR), an Energy Frontier Research Center funded by the US Department of Energy, Office of Science, Basic Energy Sciences under award no. DE-SC0019381. This research used resources of the National Energy Research Scientific Computing Center (NERSC), a US Department of Energy Office of Science User Facility operated under contract no. DE-AC02-05CH11231. Use of the Center for Scientific Computing at UC Santa Barbara supported by the National Science Foundation (NSF) Materials Research Science and Engineering Centers program through NSF DMR 1720256 and NSF CNS 1725797 is also acknowledged.

Author contributions

All of the authors participated in the analysis of data and preparation of the manuscript. First-principles calculations were performed by M.D.R. and J.V.

Competing interests

The authors declare no competing interests.

Additional information

Supplementary information is available for this paper at https://doi.org/10.1038/s41560-019-0439-6.

Reprints and permissions information is available at www.nature.com/reprints.

Correspondence should be addressed to M.D.R. or A.V.

Publisher's note: Springer Nature remains neutral with regard to jurisdictional claims in published maps and institutional affiliations.